COMPARISON OF FISSION GAS SWELLING MODELS FOR AMORPHOUS U3SI2 AND CRYSTALLINE UO2

A Thesis
Presented to
The Academic Faculty

by

Thomas C. Winter

In Partial Fulfillment
of the Requirements for the Degree
Master of Science in the
School of Nuclear and Radiological Engineering

Georgia Institute of Technology
May 2016

COMPARISON OF FISSION GAS SWELLING MODELS FOR AMORPHOUS U3SI2 AND CRYSTALLINE UO2

Approved by:

Professor Chaitanya Deo, Advisor
School of Nuclear and Radiological Engineering
Georgia Institute of Technology

Professor Bojan Petrovic
School of Nuclear and Radiological Engineering
Georgia Institute of Technology

Professor Preet Singh
School of Material Science
Georgia Institute of Technology

Date Approved: 22 Februrary 2016

To all the people who lent a helping hand along the way.

ACKNOWLEDGEMENTS

I want to thank my advisor, Dr. Deo, for his guidance and assistance while pursuing my studies and conducting my research. I would also like to thank the rest of my thesis committee: Dr. Singh and Dr. Petrovic for their comments and encouragement.

Thank you to my friends and family for the support they have provided to help get me where I am today. Lastly, thank you to Christa Kelly for all your love and support.

This material is based upon work supported under a Department of Energy Nuclear Energy University Programs Graduate Fellowship. Any opinions, findings, conclusions or recommendations expressed in this presentation are those of the authors and do not necessarily reflect the views of the Department of Energy Office of Nuclear Energy. The UO_2 swelling outputs were possible because of previous work preparing the UO_2 models in Matlab by Hubert Gibson. This work was motivated thanks to Dr. Petrovic and the IRP grant for the I2S-LWR project.

TABLE OF CONTENTS

LIST OF TABLES

LIST OF FIGURES

SUMMARY

Theoretical models are used in support of the I2S-LWR (Integral Inherently Safe LWR) project for a direct comparison of fuel swelling and fission gas bubble formation between U_3Si_2 and UO_2 fuels. Uranium silicide is evaluated using a model developed by Dr. J. Rest[20] with the fuel in a amorphous state. The uranium dioxide is examined with two separate models developed using a number of papers. One model calculates the swelling behavior with a fixed grain radius[12] while the second incorporates grain growth into the model[12, 6, 14, 11, 2, 7]. Uranium silicide rapidly becomes amorphous under irradiation[4]. The different mechanisms controlling the swelling of the fuels are introduced including the knee point caused by the amorphous state for the U_3Si_2. The outputs of each model are used to compare the fuels.

CHAPTER I

INTRODUCTION

Uranium silicide (U_3Si_2) is being examined for the I2S-LWR project as a possible alternative to conventional fuel in a nuclear reactor. There are potentially a multitude of benefits to using U_3Si_2 as fuel over UO_2. These include high uranium density, increased thermal conductivity, a longer potential fuel cycle, and potentially favorable swelling characteristics. These characteristics are important to I2S-LWR as they lead to U_3Si_2 being an accident tolerant fuel that reacts favorably when compared to UO_2 in a loss of coolant accident (LOCA) scenario.

Theoretical models more readily allow for a direct comparison between fuels. More specifically, fuel swelling and fission gas bubble formation for U_3Si_2 and UO_2. Separate models are implemented to evaluate the fission gas bubble formation and swelling behavior of U_3Si_2 and UO_2 due to different mechanisms for bubble formation. Separate models are necessary due to ceramic versus intermetallic composition and methods of bubble formation.

If swelling is too severe then contact between the fuel and cladding may occur. When this occurs there may be a fuel-cladding chemical interaction (FCCI) or a fuel-cladding mechanical interaction (FCMI.) Both of which may lead to cladding failure. Originally it was thought that U_3Si_2 behaved similarly to UO_2 while being irradiated in that the fuel stayed in a crystalline state and models were built around this assumption. This was assumed because after undergoing irradiation, U_3Si undergoes swelling at an unacceptably high rate, which has been attributed to amorphization. Although U_3Si_2 did not undergo this extreme swelling behavior and was assumed to be crystalline like UO_2 since it has relatively small bubbles through high burnup.[20]

When models for swelling did not match experimental results, further investigation by irradiation with krypton ions showed that the fuel underwent amorphization fairly rapidly and maintained an amorphous state until high doses.[4]

The uranium silicide model, developed by Dr. J. Rest[20], with the fuel in a amorphous state was used. Since uranium silicide rapidly becomes amorphous under irradiation, the distribution of bubbles and their effects on the material differ from those of uranium dioxide. U_3Si_2 stays amorphous until a high dose because of the higher number of the stronger Si-Si bonds in U_3Si_2 relative to U_3Si.[8] These bonds also increase with burnup as Uranium is depleted. Normally under an amorphous state the diffusivity of the bubbles are much higher and, when combined with the plastic flow rate of the fuel, lead to excessive swelling. In the case of U_3Si_2, the Si-Si bonds overcome these effects. In U_3Si there is a dramatic increase in free volume, while U_3Si_2 contracts upon amorphization reducing free volume.[5] In the amorphous state, bubble nucleation sites are distributed uniformly and take on the free volume that is created when U_3Si_2 contracts upon amorphization.

Another beneficial factor affecting the swelling behavior of U_3Si_2 is that the solubility of the fission gas atoms increases with fuel burn-up. The mechanism for this is an increase in Si-Si bonds relative to the weaker U-Si bonds as the uranium in the fuel is spent reducing the U to Si fraction. Due to the increase in the stronger Si-Si bonds the diffusivity for the fission gas atom decreases trapping more gas atoms in solution.[5]

Initially all bubbles are assumed to be distributed uniformly. Bubbles grow as gas atoms diffuse to the bubbles. As the bubbles begin to grow their lognormal size distribution has a peak of smaller bubble and a tail of larger bubbles. As they continue to grow larger, bubbles begin to coalesce. Eventually, bubbles in the tail reach a size where they, on average, coalesce with one other bubble. This point is known as the knee point and is where swelling accelerates due to the increase in bubble coalescence.

The number of bubbles then decreases and the distribution shifts to larger bubbles as they continue to grow and repeat the coalescence process.

In UO_2 the nucleation sites are at vacancies and the bubbles are concentrated at grain boundaries. Vacancies are created due to irradiation and gas diffusion is dependent on vacancy migration. The gas diffusion is dependent on three parts; intrinsic diffusion at high temperatures, vacancy assisted diffusion dependent on both temperature and fission rate, and irradiation enhanced athermal diffusion[12, 3]. In addition to intragranular bubbles, there are intergranular bubbles at the grain boundaries. Over time as intragranular bubbles and gas atoms accumulate on the grain boundaries, the intergranular bubbles grow and cover the grain faces. Eventually they interconnect along the grain boundaries, which can lead to fission gas release when the interconnection reaches the surface. For UO_2, one model calculates the swelling behavior with a fixed grain radius[12] while the second incorporates grain growth into the model[12, 6, 14, 11, 2, 7]. In the grain growth model swelling happens similarly, but they are accumulated into the grain face as the grain faces sweep across intragranular bubbles.

CHAPTER II

THEORY

2.1 U_3Si_2

The U_3Si_2 amorphous model was developed from a previously published model by Rest[20]. The model describes the formation and behavior of fissions gases in an irradiated amorphous material. In the model, small gas atom clusters nucleate into bubbles at shear bands surrounding free volume regions. When a crystalline material is damaged during irradiation vacancies can be formed, but in an amorphous material free volume is formed. Similar to how bubbles will nucleate at vacancy sites in crystalline materials, in amorphous materials they form at the free volume. These initial bubbles are then susceptible to re-solution due to the stress from the plastic flow of material around the free volume. The diffusivity, D_g, of the gas in an amorphous material can be described by,

$$D_g = \frac{kT}{6\pi r_g \eta} \tag{1}$$

where k is the Boltzmann's constant, T is temperature in K, r_g is the gas atom's radius, and η is the viscosity. The viscosity is inversely proportional to the fission rate $\dot{f}$,

$$\eta = \frac{\eta_0}{\dot{f}} \tag{2}$$

Where η_0 is temperature dependant, $\eta_0 = e^{-\theta/T}$. To get obtain a diffusivity with a fission rate dependency we can substituting Eq. (2) into Eq. (1) to obtain Eq. (3),

$$D_g = \frac{kT\dot{f}}{6\pi r_g \eta_0} = D_0 \dot{f} \tag{3}$$

Where $D_0 = \frac{kT}{6\pi r_g \eta_0}$. Bubbles can also diffuse from free volume migration by a volume diffusion action. The gas bubble diffusivity then becomes

$$D_b = \frac{3\Omega D_g}{4\pi r_b^3} \tag{4}$$

Where Ω is the atomic volume and r_b is the bubble radius.

Bubbles are formed when multiple gas atoms come together and is therefore dependent on their interaction rate. These newly formed bubbles are then also susceptible to re-solution due to forces from the nearby materials caused by the strain generated when the bubble forms. For these bubbles to form there must be free volume nearby. For there to be free volume there must be an external source to cause sufficient shear stress to generate the free volume. Thus bubble formation occurs where there are shear bands which for the case of interest here may be caused by irradiation.

In a control volume of the material that is shearing at a fixed rate of γ_0, the shear creates a separation of flow in the material into shear bands that cover a fraction of the control volume f_s. Note that there must be adequate f_s or volume fraction of shear bands in the material (caused by radiation) to nucleate bubbles.

$$f_s \dot{\gamma_b} + (1 - f_{s)})\dot{\gamma_m} = \dot{\gamma_0} \tag{5}$$

Assuming $\dot{\gamma_m} \ll \dot{\gamma_0} \ll \dot{\gamma_b}$, solving for f_s in Eq. (5) becomes

$$f_s \approx \frac{1}{\dot{\gamma_b}}(\dot{\gamma_0} - \dot{\gamma_m})) \approx \frac{\dot{\gamma_0}}{\dot{\gamma_b}} = \frac{\alpha}{\dot{f}} \tag{6}$$

The shear strain rate $\dot{\gamma_b}$ in Eq. (6) is due to mechanical deformation and is assumed to be proportional to the fission rate with α as the constant of proportionality. When gas atoms come together to form bubbles the plastic flow generates shear forces opposing that formation so that the cluster must grow to a critical number of gas atoms to prevent re-solution. It is assumed that the probability that the cluster

stays intact is proportional to the viscosity. The viscosity decreases as the fission rate increases according to Eq. (2). This causes the shear strain rate in the shear bands to increase and Eq. (6) shows that an increase in $\dot{\gamma}_b$ results in a decrease in f_s. Therefore the bubble nucleation rate is proportional to f_s and the viscosity, but has an inverse squared relation to the fission rate.

$$\frac{\mathrm{d}c_b(t)}{\mathrm{d}t} \approx f_s \eta \tag{7}$$

where c_b is the gas bubble concentration.

As the initial nucleated bubbles grow and coalesce into larger bubbles and as smaller bubble are destroyed by fission fragments the bubble size distribution is coarsened. The rate equations to describe the time evolution of the fission gas in an amorphous material is analogous to the equations for a crystalline material[22],

$$\frac{\mathrm{d}c_g(t)}{\mathrm{d}t} = \beta \dot{f} - \frac{4\pi f_n D_g c_g(t) c_g(t)}{\dot{f}^2} - 4\pi r_b(t) D_g c_b(t) c_g(t) + 2b m_b(t) c_b(t) \tag{8}$$

$$\frac{\mathrm{d}c_b(t)}{\mathrm{d}t} = \frac{4\pi f_n D_g c_g(t) c_g(t)}{m_b(t)\dot{f}^2} - 16\pi r_b(t) D_b(t) c_b(t) c_b(t) - b c_b(t) \tag{9}$$

$$\frac{\mathrm{d}m_b}{\mathrm{d}t} = 4\pi r_b(t) D_g c_g(t) + 16\pi r_b(t) D_b(t) m_b(t) c_b(t) - b m_b(t) \tag{10}$$

where m_b is the number of gas atoms in a bubble of radius r_b, b is the gas atom re-solution rate, $f_n = 4\alpha\eta_0 r_g$, c_g is the concentration of gas atoms, and c_b is the concentration of gas bubbles. The values m_b, c_g, and c_b are average values at a given time. The relation between r_b and b can be see using the van der Waals gas law,

$$\frac{2\gamma}{r_b}\left(\frac{4}{3}\pi r_b^3 - b_v m_b\right) = m_b k T \tag{11}$$

where b_v is the van der Waals constant and γ is the surface tension. Looking at Eq. (8), the four terms on the right side represent the gas atoms from fission, loss of gas

atoms to bubble nucleation, loss of gas atoms to diffusion into bubbles, and gas atom gain from bubble re-solution. Similarly for Eq. (9) the three terms represent bubble gain from nucleation, bubble loss to coalescence, and bubble loss to re-solution. The right hand side of Eq. (10) represents the gain of gas atoms per bubble due to gas atom diffusion, gain per bubble from bubble coalescence, and loss per bubble from bubble re-solution. The values $c_b(t)$, $c_g(t)$, $m_b(t)$, and $r_b(t)$ can be found by numerically solving Eq. (8-11). The gas atom re-solution rate is proportional to the fission rate,

$$b = b_0 \dot{f} \tag{12}$$

Due to the effects of gas atom re-solution, bubbles initially stay in the nanometer range until the concentration is sufficient that bubbles begin to coalesce. Thus the concentration of bubbles rapidly increases at the onset of irradiation and longer times increases at a greatly reduced rate (because they are coalescing) which will allow us to set the left hand side of Eq. (9) to 0 and to drop the last term on the right hand side. Later the larger bubbles in the tail of the distribution begin to contact the more numerous smaller bubbles. This causes a spike in bubble coalescence and subsequently a spike in swelling which defines the knee point.

If we approximate the solution for Eq. (8) to be

$$c_g = \beta_e \dot{f}^{3/2} t \tag{13}$$

Then we can solve for $c_b(t)$ in terms of $m_b(t)$ and t

$$c_b = \frac{4\pi f_n D_0 \dot{f} \beta_e^2 t^2}{b_0 m_b(t)} \tag{14}$$

This is more accurate at longer times due to the assumption that the concentrations of bubble increases much slower after the initial rapid increase. If we also set

the insides of the parenthesis of Eq. (11) to 0 we can then solve for the size of bubbles in the nanometer range.

$$r_b(t) = \left(\frac{3b_v m_b(t)}{4\pi}\right)^{1/3} \tag{15}$$

If we neglect the last term in Eq. (10) and combine it with Eq. (15) we can get

$$\frac{\mathrm{d}r_b(t)}{\mathrm{d}t} = \frac{b_v D_0 \dot{f}^{5/2} \beta_e t}{r_b(t)} - \frac{b r_b(t)}{3} \tag{16}$$

Using Eq. (12) we can then integrate and solve for r_b to obtain

$$r_b = \left(\frac{3\beta_e b_v D_0 \dot{f}^{3/2} t}{b_0}\right)^{1/2} \tag{17}$$

By combining Eq. (13), Eq. (15), and Eq. (17) the solution for c_b can now be written as

$$c_b = \frac{f_n}{\dot{f}^{5/4}} \sqrt{\frac{b_0 \beta_e t}{3 b_v D_0}} \tag{18}$$

Now we will introduce the variable R_{ds} which is the ratio of bubble diameter to interbubble spacing. In a homogenous, isotropic distribution of bubbles this would be one. For the conditions we will be examining, the distribution is not homogenous and thus the value will be less than 1. This ratio is given by

$$R_{ds} = 2 r_b c_b^{1/3} \tag{19}$$

Combining Eq. (17), (18), and (19) we obtain

$$R_{ds} = 2\left(\frac{3 f_n D_0 \beta_e^2 \dot{f} b_v t^2}{b_0}\right)^{1/3} \tag{20}$$

Now to find the ratio that the knee point is met, R_{ds}^{crit}, we solve for the fission density at which this occurs as

$$(\dot{f}t)_{\mathrm{knee}} = \left(\frac{b_0}{24 f_n D_0 b_v}\right)^{1/2} \frac{\sqrt{\dot{f}}}{\beta_e} (R_{\mathrm{ds}}^{\mathrm{crit}})^{3/2} \tag{21}$$

The fraction of fission gas that is in bubbles versus in solution is given by

$$\chi(t) = \frac{m_b(t)c_b(t)}{\beta \dot{f} t} \tag{22}$$

or

$$\chi(t) = \frac{4\pi f_n D_0 \beta_e^2 t}{b_0 \beta} \tag{23}$$

The solving at the knee point gives

$$\chi_{\text{knee}} = \frac{4\pi f_n D_0 \beta_e^2 (\dot{f}t)_{\text{knee}}}{b_0 \beta \dot{f}} \tag{24}$$

With respect to R_{ds}^{crit}

$$\chi_{\text{knee}} = \frac{2\pi \beta_e (R_{\text{ds}}^{\text{crit}})^{3/2}}{\beta} \sqrt{\frac{f_n D_0}{6\dot{f} b_v b_0}} \tag{25}$$

Rest[20] shows that we find the number of bubbles at the knee point to be given by

$$N_{\text{tot}} = \int_0^\infty n(r)\mathrm{d}r = \int_0^\infty \frac{2b_v \chi \beta \dot{f} t}{\pi^{3/2}} \kappa^{5/2} r \exp\left[-\kappa r^2\right] \mathrm{d}r = \frac{b_v \chi \beta (\dot{f}t)_{\text{knee}}}{\pi^{3/2}} \kappa^{3/2} \tag{26}$$

Where $\kappa = \kappa(t) = b_0/2\beta b_v D_g t$ and the average size of the bubbles at this time is

$$\bar{r} = \frac{1}{N_{\text{tot}}} \int_0^\infty r n(r)\mathrm{d}r = \frac{1}{2}\sqrt{\frac{\pi}{\kappa}} \tag{27}$$

and R_{ds} at this time is equal to

$$R_{ds} = 2\bar{r} N_{tot}^{1/3} = (b_v \chi \beta \dot{f} t)^{1/3} = \left(\frac{\chi b_0}{2 D_0 \kappa}\right)^{1/3} \tag{28}$$

The following table list the inputs used to produce the swelling data for U_3Si_2 unless otherwise stated (varying temperature and fission rate.)

Table 1: U_3Si_2 Swelling Model Variables and Constants

Symbol	Description	Units	Value	Reference
Temp	Temperature	K	Input	
k_b	Boltzmann Constant	$(m^2kg)/(s^2K)$	1.3806×10^{-23}	
r_g	Radius of diffusing gas atom	m	0.216×10^{-9}	[21]
$\dot{f}$	Fission Rate	$m^{-3}s^{-1}$	1.7×10^{20}	
$\dot{f}_0$		$m^{-3}s^{-1}$	1.25×10^{20}	[20]
η_0	$e^{-\theta/Temp}$	kg/(m s)	$2 \times 10^6 \dot{f}_0$	[20]
b_0	Initial gas atom re-solution rate	m^3	2×10^{23}	[16]
β_e		$m^{3/2}s^{1/2}$	5.6×10^{-12}	[20]
β_v	Van der Waals Constant	m^3	$\frac{5.16\times10^{-5}}{6.023\times10^{23}}$	
α	Constant of proportionality	$m^{-3}s^{-1}$	$5 \times 10^{-10} \dot{f}_0$	[20]
f_n		kg $m^{-6}s^{-3}$	$4\alpha\eta_0 r_g/0.1$	[20]
β	Gas atoms produced per fission		0.25	[18]
γ		J m^{-2}	0.7	[4]
ϕ	Experimental time constant	s^{-1}	8×10^{-8}	[20]
β_s	Solid fission product swelling	m^3	1.75×10^{-29}	[20]

First t_{knee} is solved analytically before running the Matlab model to calculate the swelling at the knee with the appropriate equations and then again for after the knee point. I(r) is the average number of bubbles a bubble of radius r contact with and r_I is the smallest bubble in the tail of the bubble size distribution. I(r_I) is when I(r) is equal to one and r is equal to r_I. This is when the larger bubbles in the distribution will begin to rapidly coalesce with smaller bubbles. This is known as the knee, named after the increase in the slope of the swelling and is when a bubble of radius r_I intersects with on average one other bubble. Or that all bubbles in the tail of the bubble distribution participate in bubble coalescence (since r_I is the smallest

bubble in the tail.) Rest[20] shows that from the bubble size distribution in Eq. (26) and from Eq. (28) we can find

$$I(r_I) = \frac{R_{ds}^3}{6\pi^{1/2}} \left(4\sqrt{\frac{\chi b_0}{D_0} \frac{r_I^2}{R_{ds}^3}} \left(3 + \frac{\chi b_0}{D_0} \frac{r_I^2}{R_{ds}^3} \right) + \sqrt{\pi} \left(3 + 6\frac{\chi b_0}{D_0} \frac{r_I^2}{R_{ds}^3} \right) \right) \tag{29}$$

r_I is also defined as $3.33r_p$ or the peak of the size distribution described in Eq. (28). Solving for R_{ds} in Eq. (29) we find, for the values in Table 1, R_{ds} to equal 0.42.

The bubbles are broken into two groups, a large and a small group. Each group is characterized by the average bubble radius and the number density of the bubbles. At the knee point the large group, or the tail of the distribution, begins to contact the more numerous smaller bubbles and as a result the larger bubbles grow and the population of smaller bubbles is reduced. The radius at the peak of size distribution of bubbles is defined as

$$r_p = \sqrt{\frac{1}{2\kappa}} \tag{30}$$

With r_I being the smallest radius in the tail of the distribution, it is the boundary between these two groups. The larger group or the tail is centered at the bubble radius

$$r_t = 5r_p \tag{31}$$

Integrating $n(r)$ over the two groups to obtain the total amount of gas in bubbles in each group and then r_p and r_t can be fitted to be in agreement with the number of gas atoms in the bubbles of these respective sizes.

$$N_1 = \frac{1}{m(r_p)} \int_0^{r_I} m(r)n(r)\mathrm{d}r = 3.6\chi b_v \beta \dot{f} t \left(\frac{\kappa}{\pi} \right)^{3/2} \tag{32}$$

$$N_2 = \frac{1}{m(r_t)} \int_{r_I}^{\infty} m(r)n(r)\mathrm{d}r = 2 \times 10^{-3} \chi b_v \beta \dot{f} t \left(\frac{\kappa}{\pi} \right)^{3/2} \tag{33}$$

Plotting the bubble size distribution, or $n(r)$, at 473K, a fission rate of $2.5 \times 10^{20}\mathrm{m}^{-3}\mathrm{s}^{-1}$, and at the onset of the knee gives us Fig. 1.

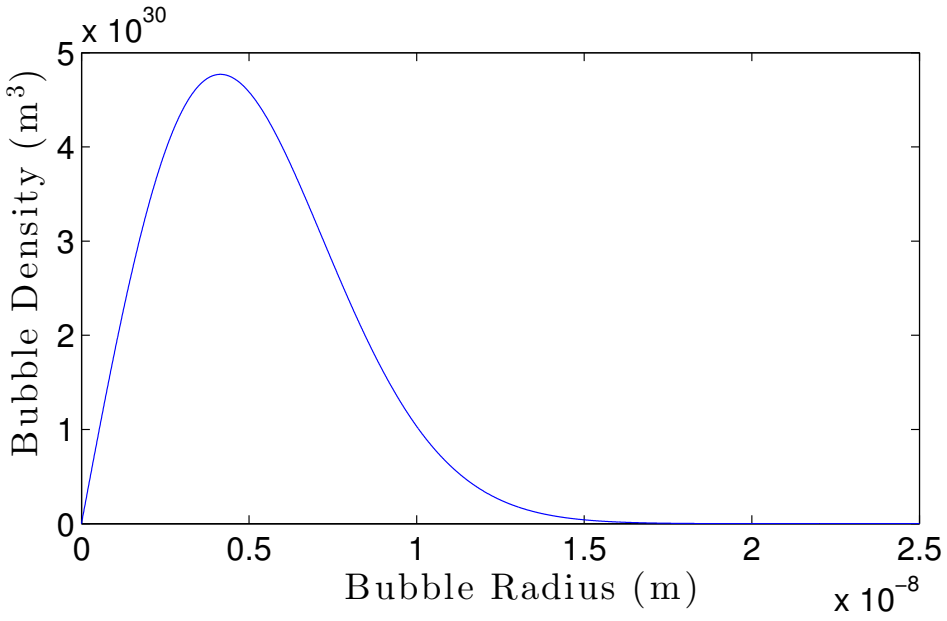

Figure 1: Bubble size distribution at the knee point with a fission rate of $2.5 \times 10^{20}\mathrm{m}^{-3}\mathrm{s}^{-1}$ and at 473K

Consider that while bubbles in the larger group are growing and absorbing bubbles in the smaller group that the number density of larger bubbles is fixed, but the number density of the smaller group is decreasing. Therefore the average radius of the large group is increases while the smaller group is fixed at r_p. This means that the gas atoms per bubble is fixed in the smaller group but increasing in the larger group. If the smaller group (N_1) loses ΔN_1 bubbles to the larger group (N_2) then the number of atoms per bubble in the larger group increases from $m(r_t)$ to m_{obs}.

$$m_{obs} = m(r_t) + m(r_p)\frac{\Delta N_1}{N_2} \tag{34}$$

We assume that the bubble distribution behaves so that when the larger bubbles swell to consume a locally high bubble density area so that it is the only bubble in that local area and contains m_{obs} bubbles. Also that on the boundary of the high density

region that bubbles have contact with only 1/2 of the other neighboring bubbles on average when the locally high density areas are removed from $n(r)$. Or that only half of the bubbles from the small group can be absorbed by the large group.

$$\Delta N_1 = \frac{N_1}{2} \tag{35}$$

Below you can see the formation and evolution of the bubbles.

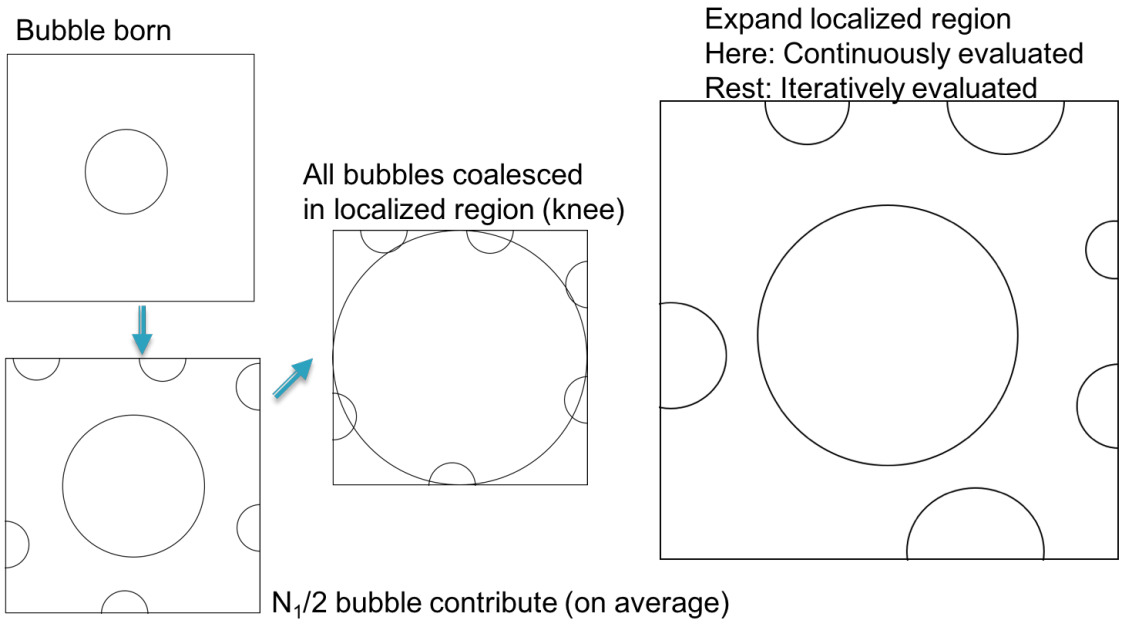

Figure 2: U_3Si_2 Bubble formation and evolution

Here we diverge from Rest's model where Rest treats the knee point as an iterative process versus here where we will consider an initial knee and then implement the effects of the knee continuously for each time step. Up to the knee point we will calculate swelling based on the initial bubble population. So we will have two time regimes, one before the knee point and one after.

$$\left(\frac{\Delta V}{V_0}\right)_{bubbles}^{t \leq t_{knee}} = \frac{4\pi}{3}\left(r_p^3 \frac{N_1}{2} + r_t^3 N_2\right) \tag{36}$$

We then include the contribution of solid fission products.

$$\left(\frac{\Delta V}{V_0}\right)^{t\leq t_{knee}} = \frac{4\pi}{3}\left(r_p^3\frac{N_1}{2} + r_t^3 N_2\right) + \beta_s \dot{f} t \tag{37}$$

After the knee point we need to consider changes to the population from the coalescence of larger bubbles during and after the knee. After the knee point larger bubbles continue to grow and coalescence with smaller bubbles. Smaller bubbles are still growing as well so effectively the bubble population is shifting to larger scales. The large bubble coalescence effects on the population are described by

$$N(t) = N_2 \ \mathrm{e}^{-\phi(t-t_{knee})} \tag{38}$$

Rest proposes that after the knee formation the fraction of gas in bubbles stays relatively constant. This supports the assumption that what gas atoms don't go into nanometer scale bubbles instead goes into the larger bubble population. Therefore the growth of the larger bubbles after the knee point is described by

$$\frac{\mathrm{d}m(t)}{\mathrm{d}t} = \frac{\beta \dot{f}\left(1-\chi(t)\right) - m(t)}{N(t)}\frac{\mathrm{d}N(t)}{\mathrm{d}t} \tag{39}$$

Using Eq. (38) and Eq. (39) can be used to obtain

$$\begin{aligned}\left(\frac{\Delta V}{V_0}\right)^{t\geq t_{knee}} &= \beta_s \dot{f} t + \frac{2\pi}{3} r_p^3 N_1 \left(1 + \frac{\chi(t)}{\chi(t_{knee})}\right) \\ &+ \left[\frac{3kT}{8\pi\gamma}\left(m_{obs} + \frac{\beta \dot{f} t \mathrm{e}^{\phi t}\left(1-\chi(t)/2\right)}{N_2}\right)\right]^{1/2}\end{aligned} \tag{40}$$

2.2 UO_2

2.2.1 UO_2 Fixed Grain Size

The models used to calculate the swelling of UO_2 were prepared by the process described in Gibson's thesis[7]. In UO_2 bubbles form at vacancies and vacancy migration leads to bubble growth. The process is less iterative than U_3Si_2 in that the grains act as sinks for the bubbles & vacancies and continue to grow as the intragranular

bubbles diffuse to the boundaries. Over time the intergranular bubbles grow causing the grain faces to grow into voids as the fuel swells. After swelling into voids, the grain faces begin to interconnect. Eventually the grain face void interconnections reach the surface and allow fission gas to escape. This is known as the saturation point. After the saturation point is reached, the fission gas is allowed to escape. This process can be seen below.

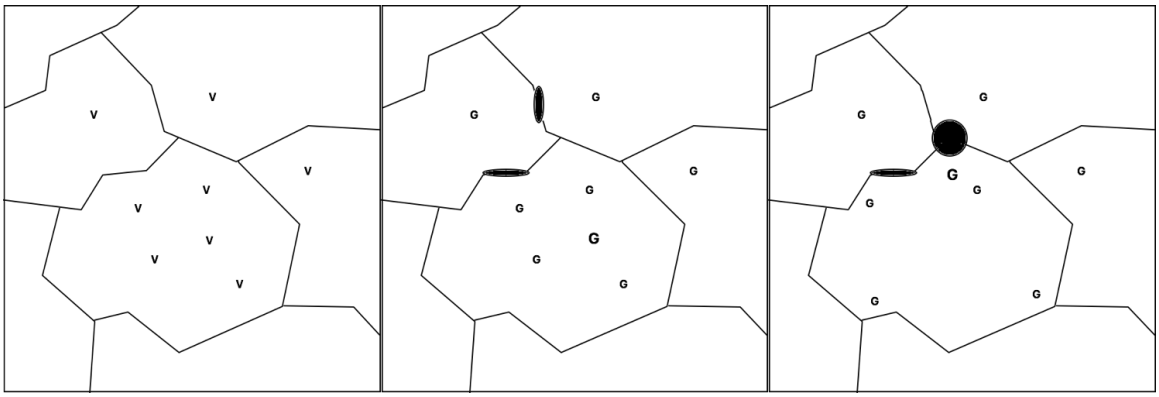

Figure 3: UO_2 Bubble formation and evolution

Table 2: UO_2 Swelling Model Variables and Constants [7, 23, 15, 24, 25, 13, 6]

Symbol	Description	Units	Value
T	Temperature	K	
k_b	Boltzmann constant	$\frac{m^2 kg}{s^2 K}$	1.3806×10^{23}
P	External pressure	Pa	10^6
t	Time	s	
t_s	Time step	s	3600
R	Grain radius	m	7.5×10^{-6}
r_{bs}	Average intergranular bubble radius at saturation	m	10^{-6}
cgb	Composite Gas Bubble Parameter [7]	m	7.25×10^{-8}
$\dot{f}$	Fission Rate	fission m^{-3}	
C_1	Constant		7.6×10^{-10}
C_2	Constant		4.5×10^{-35}
C_3	Constant		2×10^{-40}
Q_1/k_b	Activation Energy	K	35247
Q_2/k_b	Activation Energy	K	13800
L	Fission fragment range	m	6×10^{-6}
b	Van der Waals constant for Xenon		5.16×10^{-5}
δ	Damage radius of fission fragment	m	10^{-9}
$2\gamma/r_{bs}$	Surface tension to radius ratio	N/m^2	2.4×10^6

Table 3: Equations for UO_2 Swelling Model [7, 23, 15, 24, 25, 13, 6]

Symbol	Description	Equation
G_p	Gas atom production rate	$0.3\dot{f}$
G_r	Gas atom re-solution rate	$G_p(5.7 \times 10^{-8})$
D'	Diffusivity in a trap free media in UO_2	$C_1 e^{\frac{-Q_1}{k_b T}} + \dot{f} C_2 e^{\frac{-Q_2}{k_b T}} + C_3 \dot{f}$
C_b^t	Total bubble density	$\frac{1.52 \times 10^{27}}{T} - 3.3 \times 10^{23}$
$\bar{R}_b$	Intragranular bubble radius	$1.453 \times 10^{-10} \times e^{1.023 \times 10^{-3} T}$
g	Fission gas capture rate by intragranular bubbles	$4\pi \bar{R}_b C_b^t D'$
vg	Intragranular gas bubble re-solution rate	$3.03\pi LF(\bar{R}_b + \delta)^2$
D	Fission gas diffusion in UO_2	$(D'vg)/(vg + g)$
N_b	Number density of gas bubbles	$\frac{2}{3} R C_b$
κ	Ratio of bubble surface tension to exterior pressure	$2.4 \times 10^6 / P$
ν_p		(b P)/($k_b T 6.023 \times 10^{23}$)
N_{bs}	Number density at saturation	$\frac{cgb \cdot P(1+\kappa)}{k_b \cdot T(1+\nu_p(1+\kappa))}$

Over time the intergranular bubble gas density increases which leads to fuel swelling. Additionally swelling is contributed to by the intragranular fission gas bubbles and the solid fission products. The swelling from the intergranular gas bubbles stops when saturation is reached or N_{bs}. The equation for gaseous swelling is:

$$\frac{\Delta V}{V} = \frac{4\pi r_b^3 \omega_\theta N_b}{3} \tag{41}$$

In this equation r_b is the intergranular bubble radius in m, ω_θ is a geometric factor used to correct for the use of spherical bubbles with θ equal to the intergranular bubble dihedral angle, N_b is the intergranular gas bubble density in m^{-3}. The dihedral angle is assumed constant.

$$\omega_\theta = 1 - 1.5\cos(\theta) + 0.5\cos^3(\theta) \tag{42}$$

The number of gas atoms per bubble, following Van der Waals Law of gases is

$$N_{atom} = (k_b T)^{-1} (V_b - bN_{atom})(P_b + \frac{aN_{atom}^2}{V_b^2}) \tag{43}$$

Where a & b are Van der Waals constants for Xenon, aN_{atom}^2 is assumed to be negligible, V_b is the bubble volume, and P_b is the bubble pressure. The pressure of the gas bubble is [10]

$$P_b = \frac{2\gamma}{r_b} + P \tag{44}$$

Where γ is the bubble surface tension. The intergranular gas atom density and saturated density can be written as

$$C_b = \frac{4\pi}{3} r_b^3 \omega_\theta n_b \frac{P_b}{bP_b + k_b T} \tag{45}$$

$$C_{bs} = \frac{4\pi}{3} r_{bs}^3 \omega_\theta n_b \frac{P_b}{bP_b + k_b T} \tag{46}$$

or

$$C_{bs} = \frac{3N_{bs}}{2(6.023 \times 10^{23})R} \tag{47}$$

Then comparing C_b to it's saturation value, C_{bs}, the intergranular bubble radius, r_b, can be seen through the ratio of it and it's saturation value.

$$\frac{C_b(t)}{C_{bs}} = x^2 \frac{x + \kappa}{1 + \kappa} \frac{1 + (1 + \kappa)\nu_p}{1 + (1 + \kappa/x)\nu_p} \tag{48}$$

Where x is the ratio of r_b & r_{bs}, κ is the ratio of bubble surface tension to exterior pressure, and ν_p is

$$\nu_p = \frac{bP}{k_b T} \tag{49}$$

Then the volumetric swelling can be calculated through the equation below and reaches saturation when x=1 or C_b becomes C_{bs}.

$$\frac{\Delta V}{V} = \frac{k_b T \left[1 + (1 + \kappa/x)\, \nu_p\right] C_b}{P\,(1 + \kappa/x)} \tag{50}$$

2.2.2 UO_2 Grain Growth

The grain growth model is similar to the fixed grain model and both reach a saturation point where gas is allowed to escape. In addition to gas causing the grain boundaries to become voids and swell, some of the grains grow consuming neighboring grains. Therefore in the grain growth model, as some grains grow this causes other grains to shrink. As the grain faces sweep across the volume of the fuel, they pick up intragranular gas atoms and release them into the boundaries or voids. This then leads to a decrease in intragranular gas density. The addition of grain growth to the fixed grain bubble formation and evolution can be seen below.

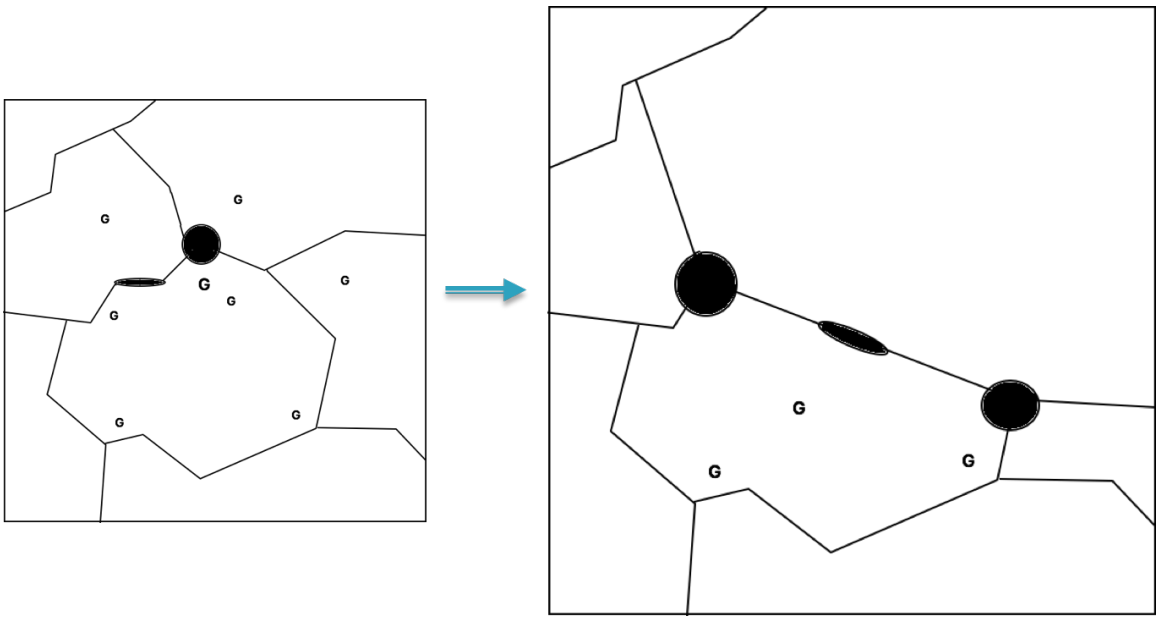

Figure 4: UO_2 Bubble Evolution with Grain Growth

The grain growth model used in Gibson's thesis [7] is developed from Jernkvist's and Massih's work [9]. The rate of grain growth is given as

$$\frac{\mathrm{d}R}{\mathrm{d}t} = \frac{k_g}{2}\left(\frac{1}{2R} - \frac{1}{D_{m,UO_2}}\right) \tag{51}$$

$$D_{m,UO_2} = D_0\left[H(T_g - T) + H(T - T_g)A_m \mathrm{e}^{-Q_m/T}\right] \tag{52}$$

$$k_{g,UO_2} = A_g \mathrm{e}^{-Q_g/T} \tag{53}$$

Where D_{m,UO_2} is the maximum grain diameter, D_0 is the initial grain diameter, k_g is a temperature dependent coefficient, T_g is 1550K, A_m is 615.59, Q_m is 9955K, A_g is 4.11×10^{-9} m s^{-}1, Q_g is 32114.51K, and H is the Heaviside step function. The step function is used to restrict grain growth to temperatures above 1550K where H equals 1 otherwise it equals 0. The grain growth formula comes from Turnbull's work[2].

CHAPTER III

RESULTS

3.1 U_3Si_2 Fission Gas Evolution

Over time the bubbles in the amorphous U_3Si_2 grow and have a distribution with a bell shaped peak and tail. At this time there is a portion of the bubbles that reach sufficient size to interact and merge with nearby bubbles. This size is when the radius of the two bubbles is greater than the interbubble distance. The interbubble distance in relation to bubble radius can be seen in the following figure.

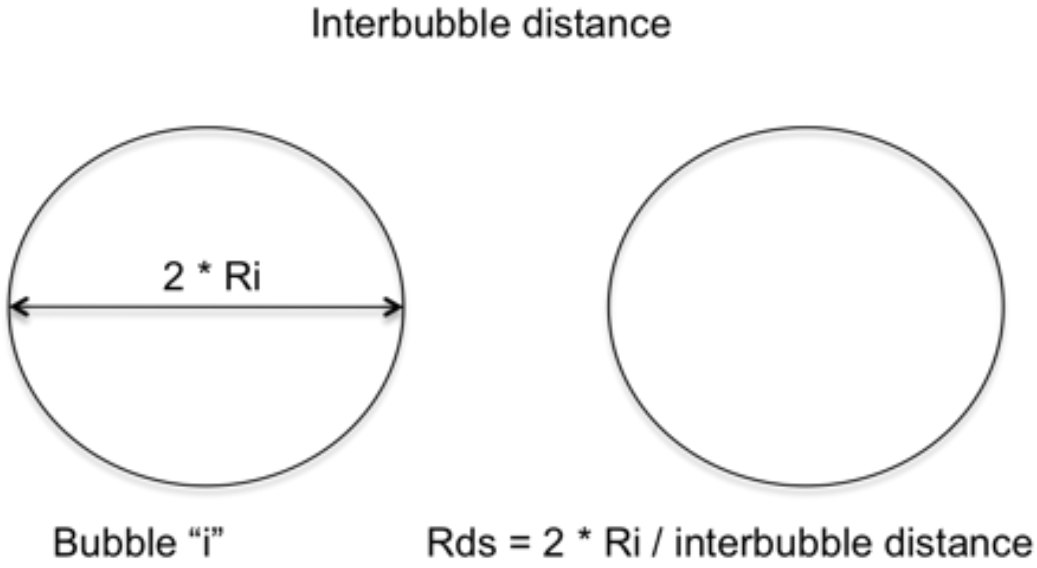

Figure 5: Interbubble Distance

In the figure below, I(r) is the average number of bubbles that a given bubble of radius r intersects with. The knee occurs when I(r)=1 and the radius is equal to r_I. In the figure, this occurs when the radius is approximately equal to 14nm.

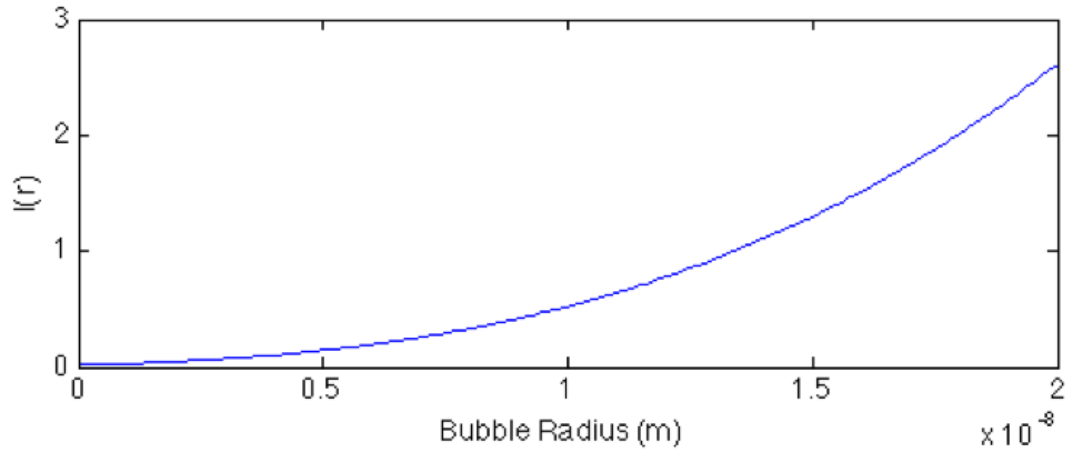

Figure 6: I(r) vs Bubble Radius: 2.5×10^{20} fissions $m^{-3}s^{-1}$ at 473K for U_3Si_2

The U_3Si_2 model exhibits the behavior where the bubbles reach radius r_I and merge at the knee point. The swelling accelerates at this point as the bubbles coalesce into a population of larger diameter bubbles.

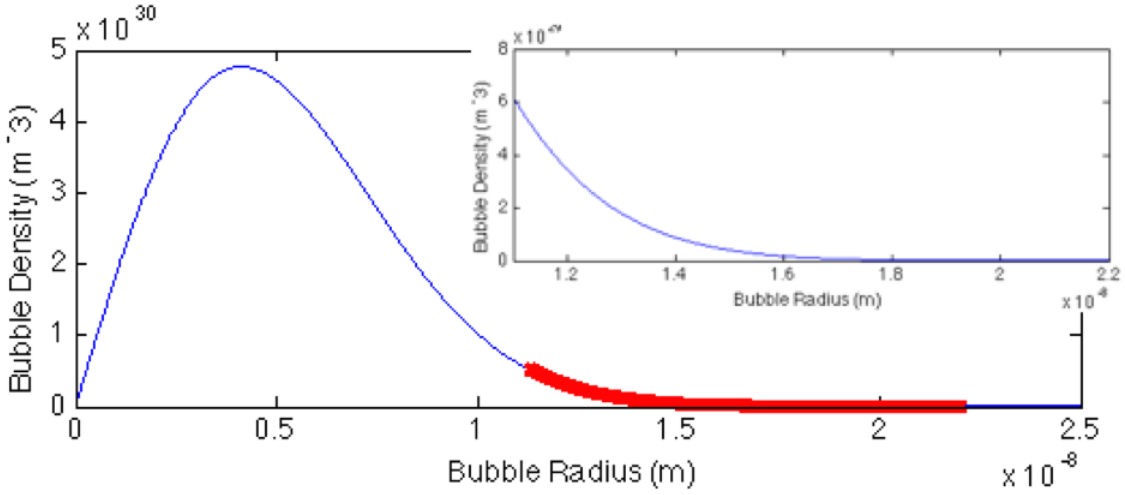

Figure 7: Bubble Density vs Bubble Radius

After the knee point time (t_{knee}) the bubbles' population decreases as bubbles coalesce and continue to grow. This continues until the distribution is again a peak

and a tail, but with a higher average radius and lower population.

Figure 8 was generated from Eq. (37) and (40) (before and after t_{knee}.) From the fractional swelling figure below we can see that at higher fission rates, the swelling is decreased for a given fission density. The swelling is decreased because there is an increase in energetic particles. These energetic particles collide with and collapse some of the smaller bubbles leading to an increase of gas in solid solution for a given fission density. The time t_{knee} can be seen in the following figure where the swelling spikes as the bubbles merge more rapidly at the knee. It is also clear that the knee point occurs at a higher fission density with higher fission rates.

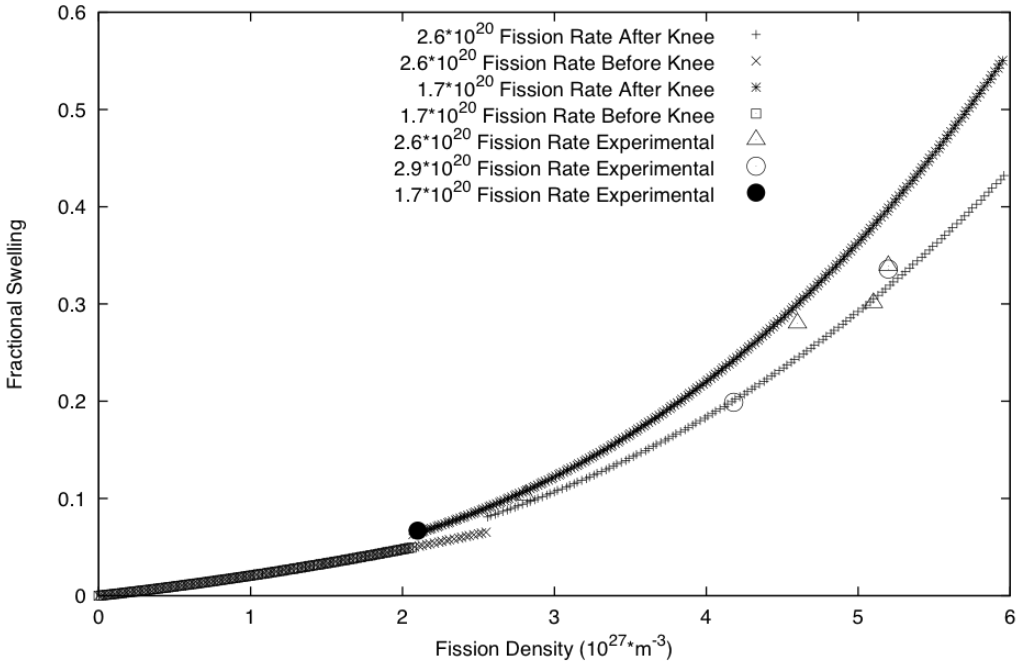

Figure 8: Fractional Swelling vs Fission Density for U_3Si_2 for various fission rates compared to experimental values

Eq. (28) is used to find R_{ds} at t_{knee}, which is then used to solve for the fission rate and fission density at t_{knee}. Eq. (21) was used to generate Figure 9. From Figure 9 it can be seen that as the fission rate increases the fission density to reach the knee point increases. This is again because more gas atoms per fission are in solid solution

due to an increased gas re-solution corresponding to the increased fission rate. Eq. (12) shows how the gas re-solution rate increases with fission rate because the fission products colliding with bubbles can cause them to collapse.

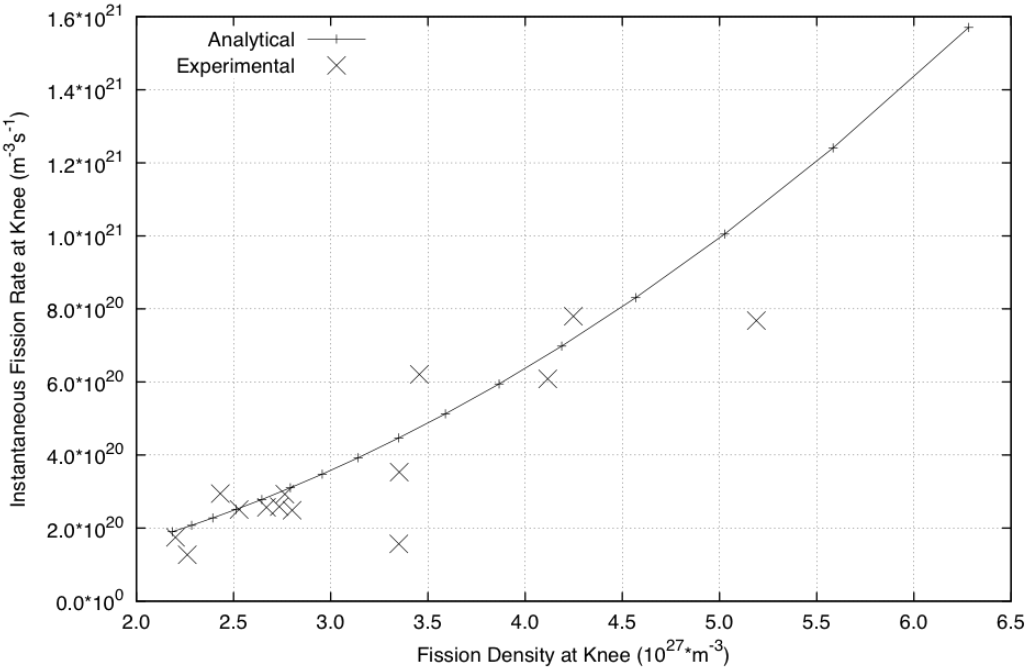

Figure 9: Fission Rate vs Fission Density at Knee: Comparison of Experimental and Analytical Values

Figure 10 is generated using Eq. (24). At higher fission rates, the χ (fraction of gas in bubbles) is lower at the knee. This is because at these higher fission rates the fission gas re-solution rate increases such that a lower fraction of gas is in bubbles. Yet the total amount of gas in bubbles still increases, albeit at a lesser degree than that with which the fission rate increases.

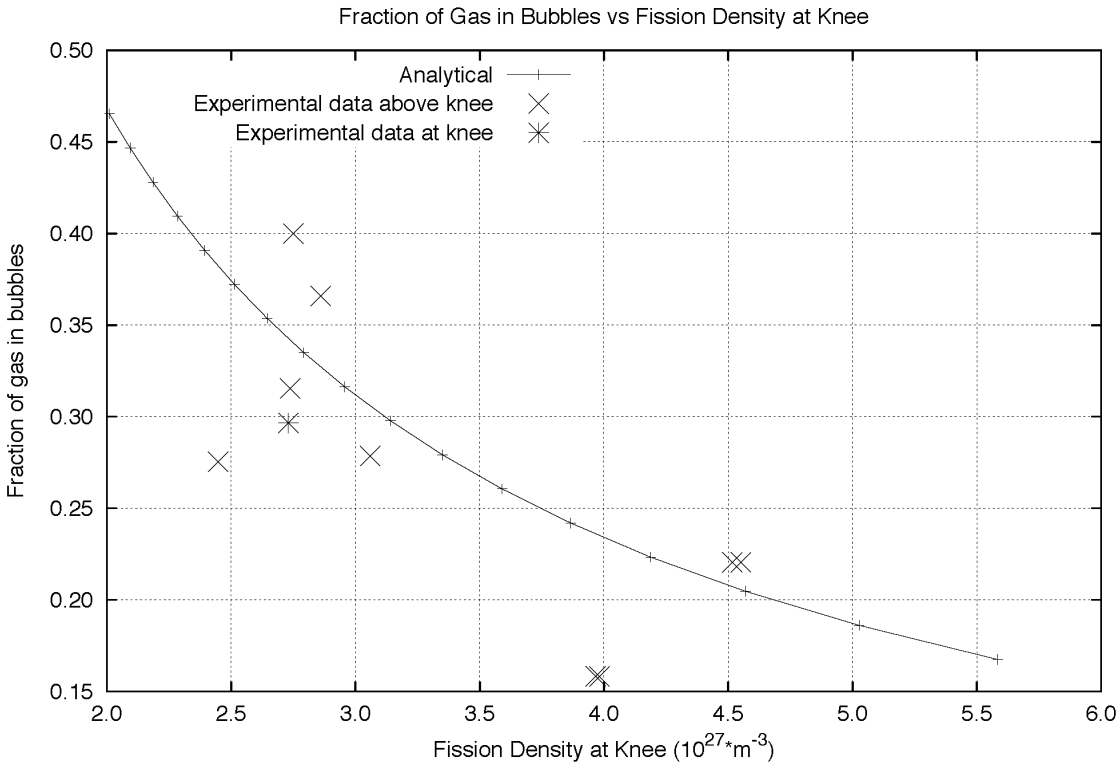

Figure 10: Fraction of Gas in Bubbles vs Fission Density at Knee

Eq. (38) describes the large bubble population evolution over time after t_{knee}. Eq. (38) is used to generate Figure 11. As the fission density increases the bubble density decreases. This is because as the number of fission gas atoms increase; the bubbles swell and then coalesce with one another and reduce the total number of bubbles. So there are fewer bubbles but the amount of gas in and subsequently the size of each bubble increases causing the swelling to increase.

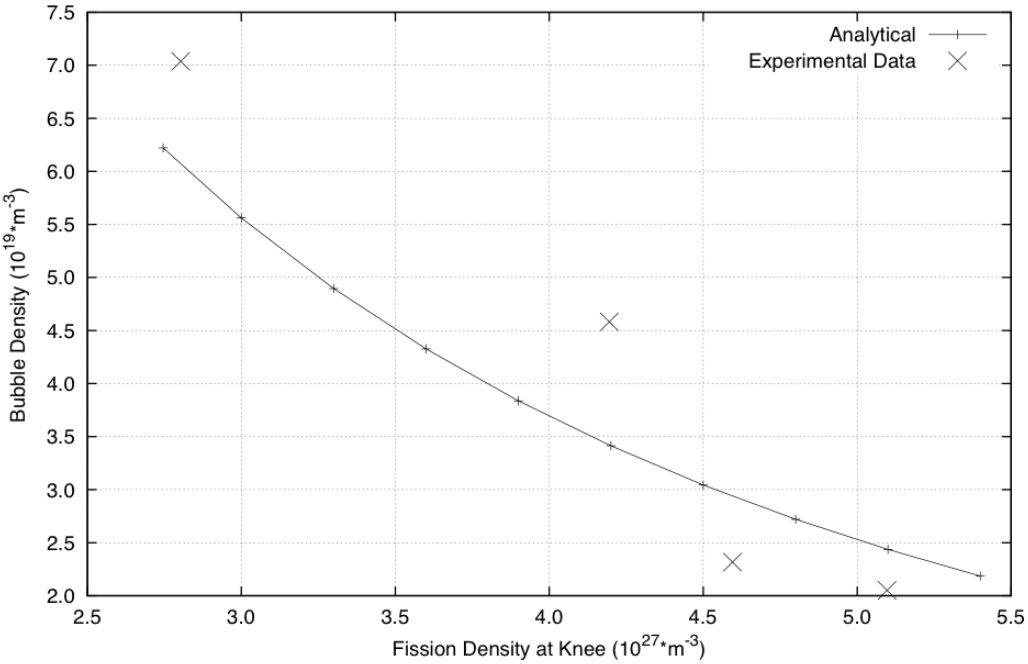

Figure 11: Bubble Density vs Fission Density after the knee point for U_3Si_2 at a fission rate of 3×10^{20} fissions $m^{-3}s^{-1}$ at 473K

3.2 UO_2

3.2.1 Fixed Grain UO_2 Fission Gas Evolution

Figure 12 shows the fractional swelling versus time for UO_2 with a fixed radius of 7.5×10^{-6} m and is generated with Eq. (49). Over time vacancies diffuse to the grain boundaries and gas atoms collect at the vacancies forming bubbles at the boundaries. These bubbles then interconnect and cover the grain face. Eventually as enough bubbles and grain faces interconnect the gas is allowed to escape to the surface and release. This is the saturation point and where gaseous swelling stops with this model.

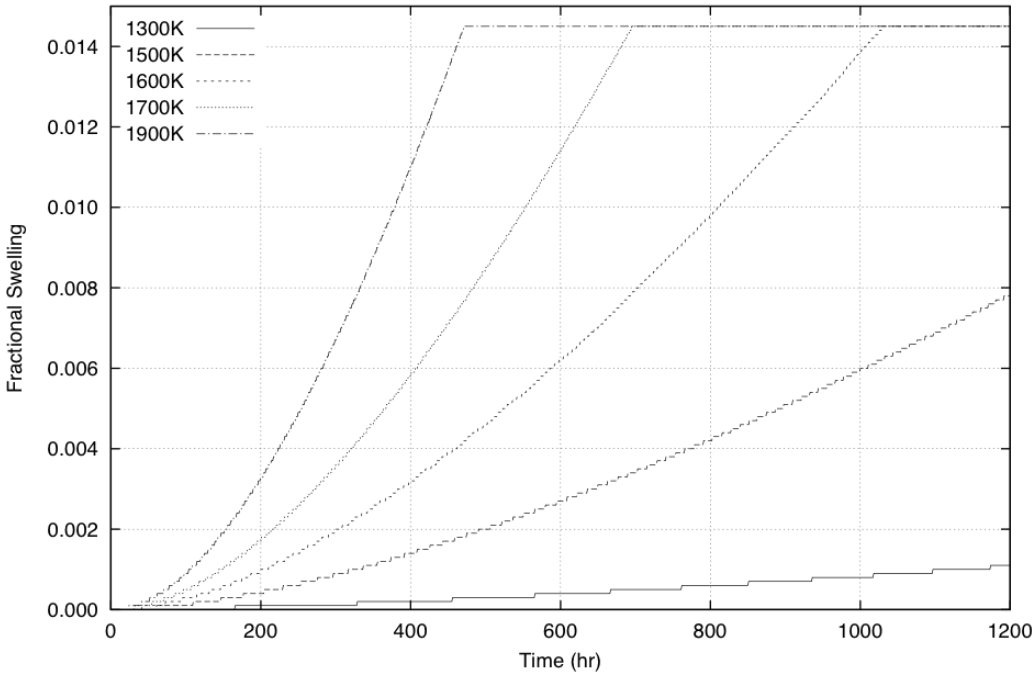

Figure 12: Fractional Swelling vs Time for UO_2 using fixed grain swelling model for grain size of 7.5×10^{-6} m at 2.5×10^{19}fissions m^{-3} s^{-1}

Figure 13 shows the bubble radius versus the saturation bubble radius. The average intergranular bubble radius for the saturation point is r_{bs} and r_b is the average intergranular bubble radius. This ratio is the value x in equation Eq. (50). The time to reach the saturation point for a given fission rate is very sensitive to the temperature. When this fraction reaches a value of one, then the saturation point is achieved. The plot indicates that as the temperature increases, the time to reach saturation decreases. This is because at higher temperatures the intragranular gas bubbles can more quickly diffuse to the grain boundary as can be seen in D' from Table 3.

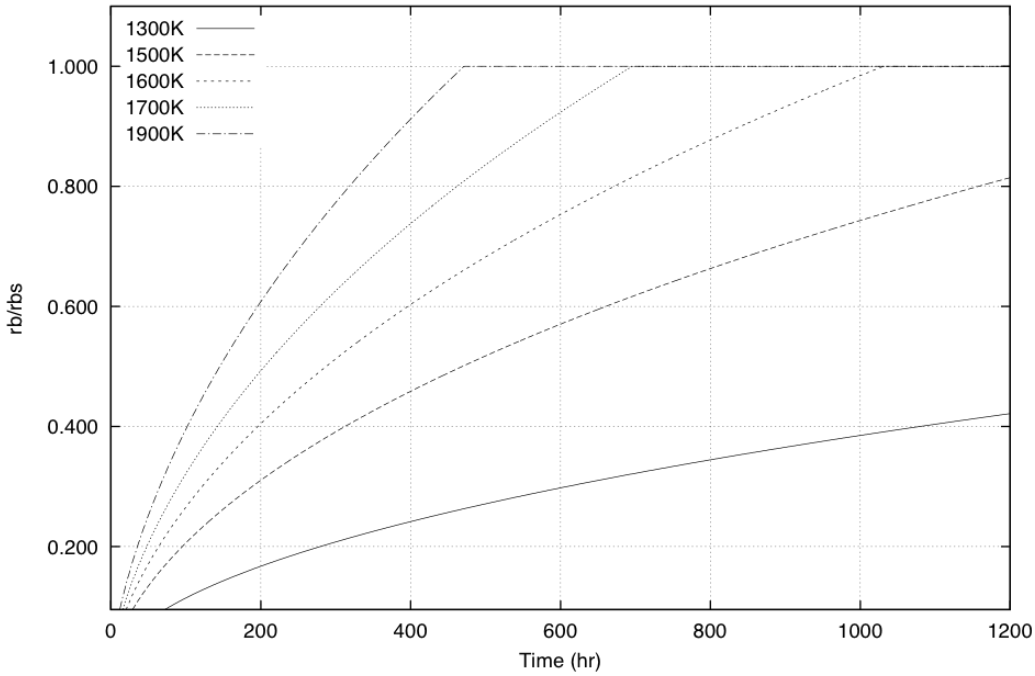

Figure 13: r_b/r_{bs} vs Time for UO_2 at various temperatures and a 7.5×10^{-6} m grain radius at 2.5×10^{19}fissions m^{-3} s^{-1}

The intergranular gas density can be seen with equations Eq. (45) and Eq. (46) which were used to produce Figure 14. At higher temperatures the gas density, or the gas atoms in intergranular bubbles per unit area of grain boundary, necessary to reach saturation decreases because the gas atoms are more energetic and form larger bubbles. This can be seen from N_{bs} in Table 3 where at the temperature increases the number of gas bubbles and thus the gas density (and time) to saturation decreases.

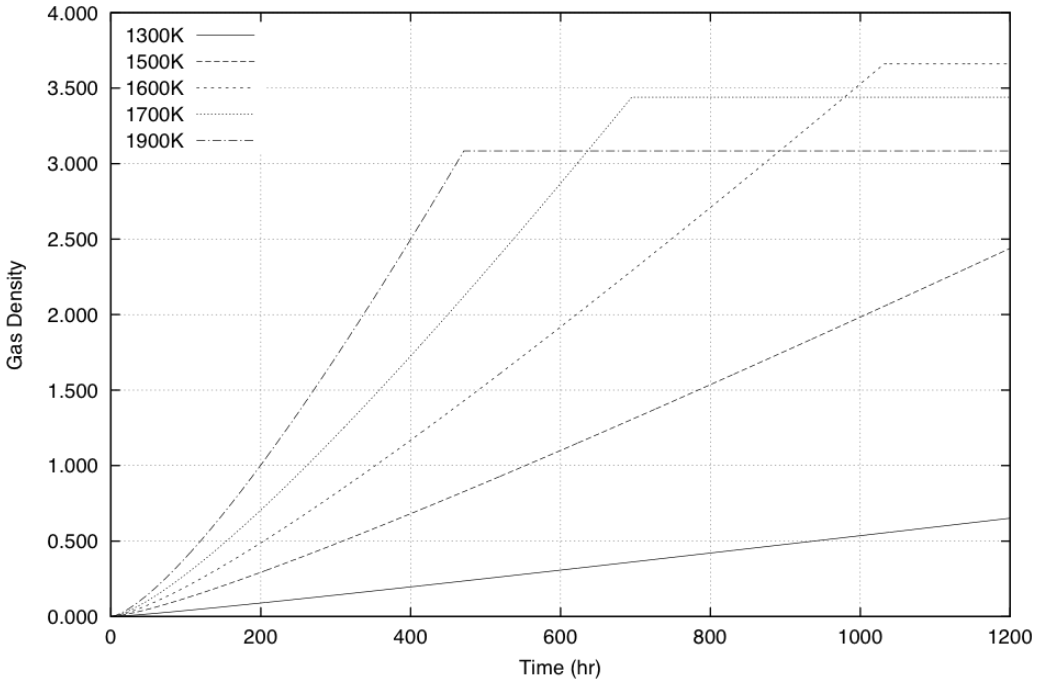

Figure 14: Intergranular Gas Density (mol m^{-3}) vs Time for UO_2 at various temperatures and a 7.5×10^{-6} m grain radius at 2.5×10^{19}fissions m^{-3} s^{-1}

Figure 15 shows the number density of gas bubbles over the number density of gas bubbles at saturation versus time. This ratio can be calculated from the ratio of the N_b and N_{bs} in Table 3. This again shows how the fission density and subsequently time to reach saturation is sensitive to temperature. This is due in part to the increased diffusion of intragranular bubbles to intergranular bubbles as seen in D' from Table 3.

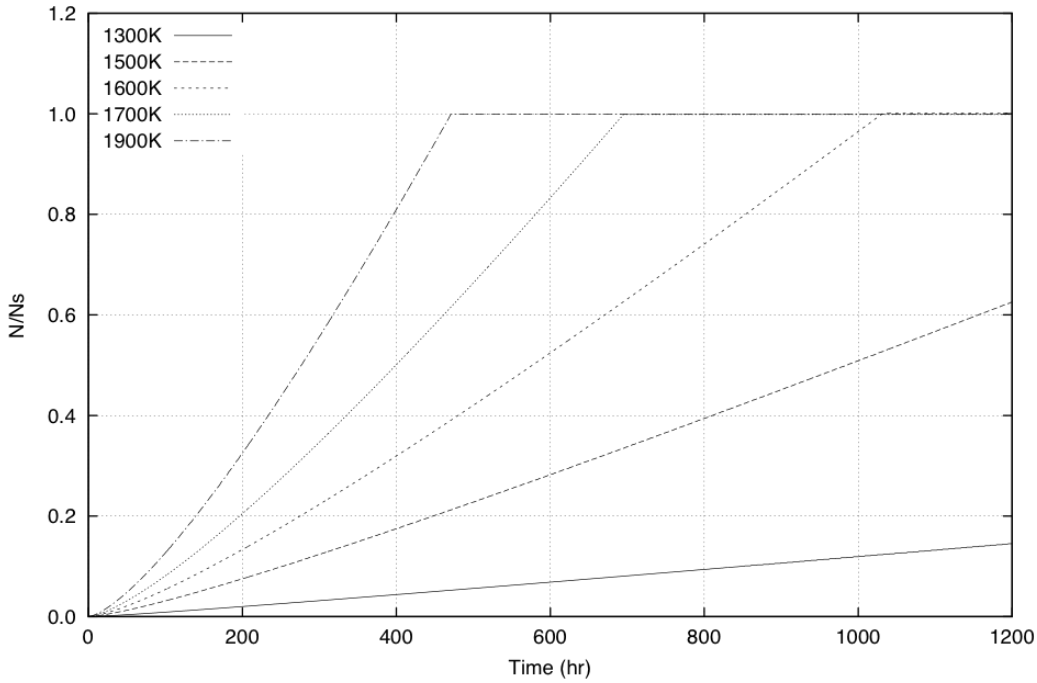

Figure 15: Fractional Gas Sat. vs Time for UO_2 at various temperatures and a 7.5×10^{-6} m grain radius at 2.5×10^{19}fissions m^{-3} s^{-1}

3.2.2 UO_2 Grain Growth Fission Gas Evolution

The Grain Growth model was run with an initial grain radius of 5×10^{-6} m at 1600K and a fission rate of 1.53×10^{19} $m^{-3}s^{-1}$. Similar to the Fixed Grain model, after the saturation point is reached the fission gas is allowed to escape. As the grain faces sweep across the volume of the fuel, they pick up intragranular gas atoms and release them. This then leads to a decrease in intragranular gas density as can be seen below in Figure 16. At higher temperatures the grains grow larger as can be seen in Eq. (52) and this causes the grain faces to sweep and release more gas leading to a lower gas density at higher temperatures.

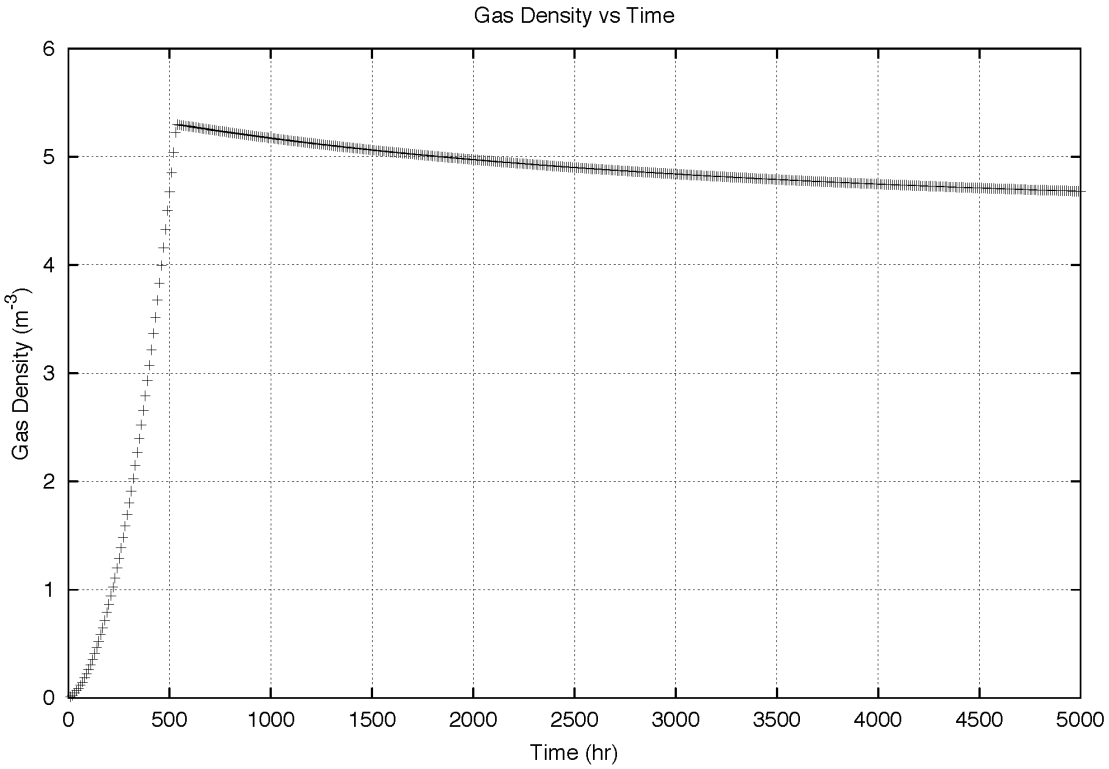

Figure 16: Gas Density vs Time for UO_2 Grain Growth Model at 1600K

The average grain size increases with time as the grain faces sweep across the fuel and lead to the number of grains decreasing. With Eq. (53) we can produce Figure 17 which shows the effect this has on the average grain size below. With Eq. (52) we can calculate that the maximum grain radius is 6.11×10^{-6} m.

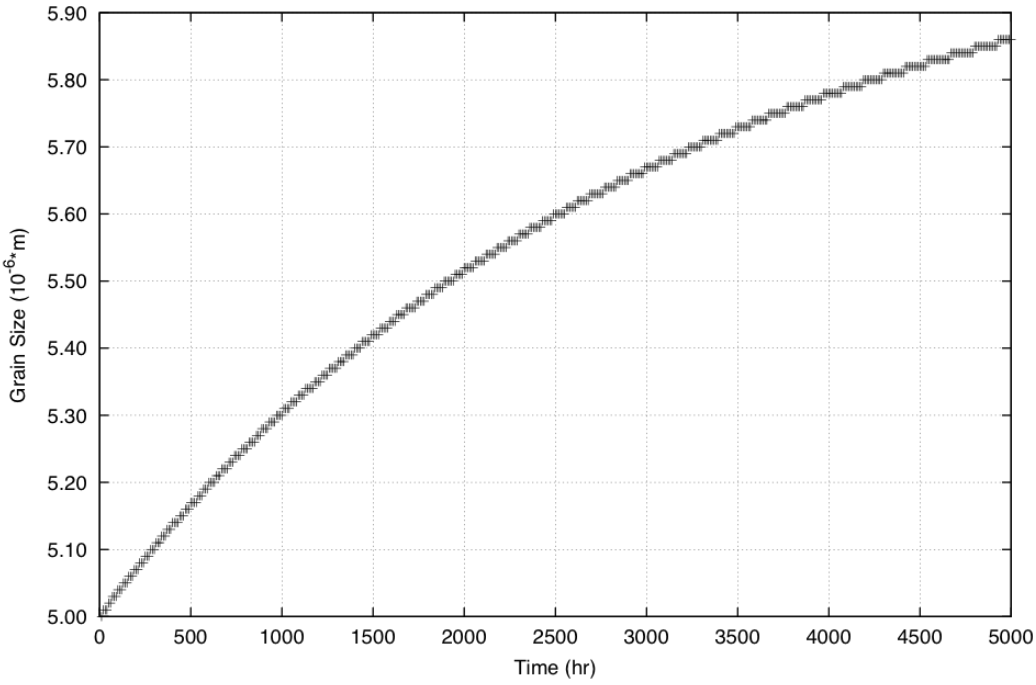

Figure 17: Grain Size vs Time for UO_2 Grain Growth Model at 1600K

As can be seen in Figure 18, compared to the fixed grain model, the saturation point is reached much more quickly due to the grain growth and grain boundaries sweeping across the fuel picking up intragranular gas atoms.

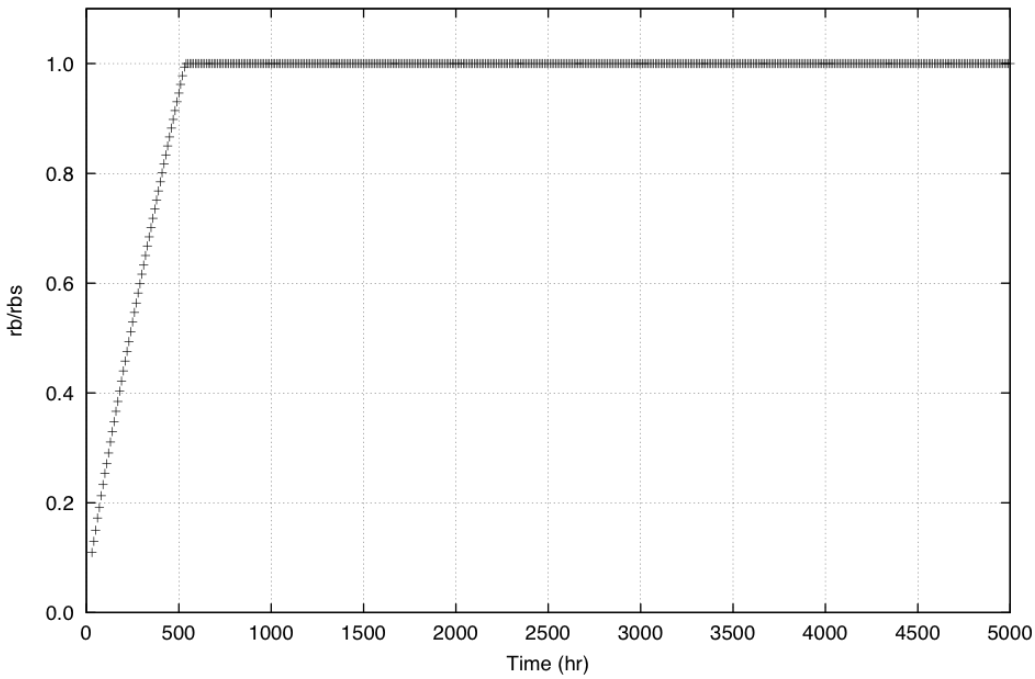

Figure 18: r_b/r_{bs} vs Time for UO_2 Grain Growth Model at 1600K

After the saturation point the swelling decreases as more gas atoms are swept over by the grain boundary. This is due to the decreases in gas density from intragranular gas atoms escaping after the saturation point is reached.

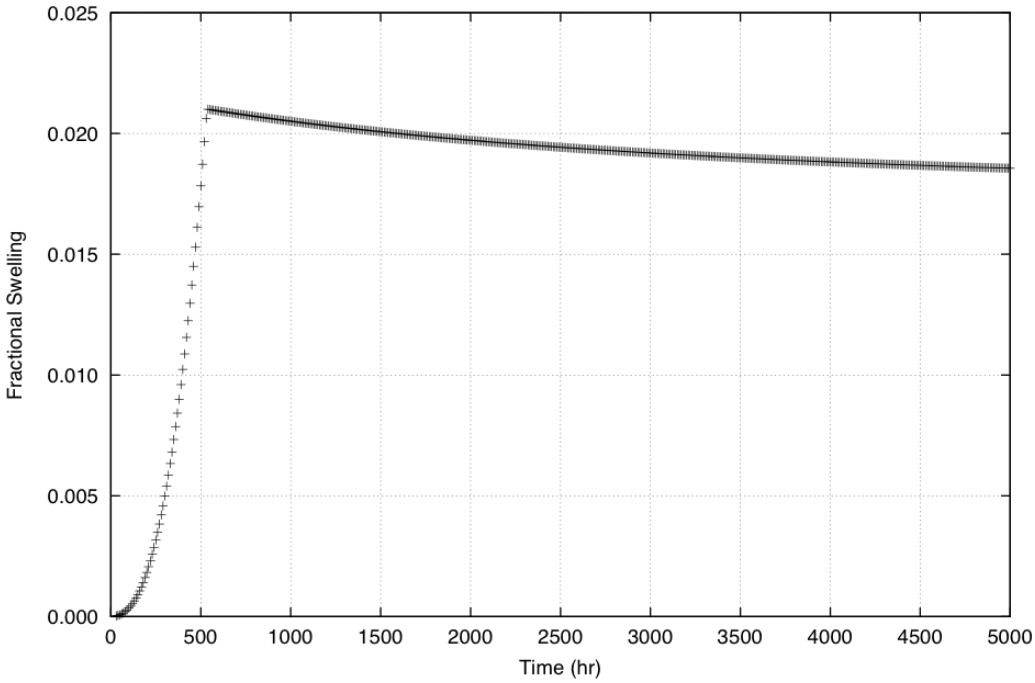

Figure 19: Fractional Swelling vs Time for UO_2 Grain Growth Model at 1600K

Another difference from the Fixed Grain model can be seen in Figure 20. The saturation point can be seen where the initial release of gas occurs. In the fixed grain model the fractional gas release stays constant as gas is uniformly born intragranular and diffusing to the voids to vent. In the grain growth model the sweeping grain faces pick up additional intragranular gas atoms increasing the fractional gas release after saturation.

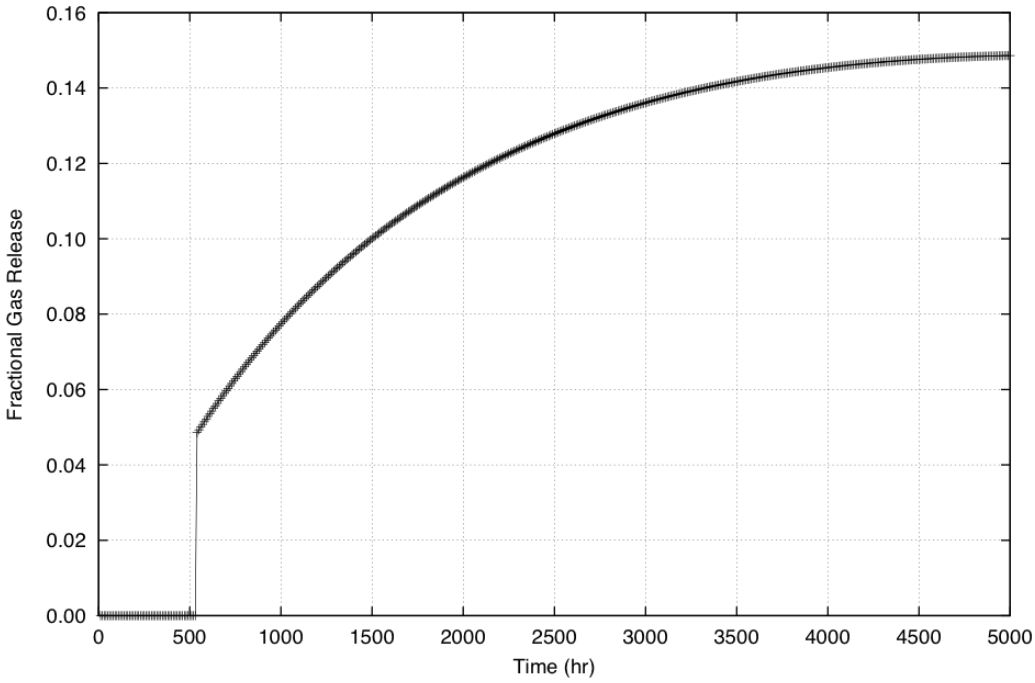

Figure 20: Fractional Gas Release vs Time for UO_2 Grain Growth Model at 1600K

CHAPTER IV

CONCLUSION

It is clear, that after the knee point, the swelling accelerates for the U_3Si_2 fuel. This should not be a problem for the I2S-LWR as the fuel should be achieving 37-46 GWd/tU[19] through its life in the reactor and the knee point should not be reached by this point. In Figure 8 the knee points occur at 2.55×10^{27} fissions m^{-3} and 2.05×10^{27} fissions m^{-3} for 2.6×10^{20} fissions m^{-3} s^{-1} and 1.7×10^{20} fissions m^{-3} s^{-1} respectively. These correspond to 85 GWd/tU and 69 GWd/tU respectively with an assumed 95% theoretical density or 10.735 gU cm^{-3}. Therefore, at these burnups for I2S-LWR, there should be minimal risk of the knee point being reached. In addition due to the higher temperature of the reactor at approximately 350°C, the fuel should not be in an amorphous state.

The fission rates expected in a power reactor or I2S-LWR are of an order of magnitude lower than those seen in the swelling already calculated for U_3Si_2 in this paper. Therefore the swelling was again calculated for 20, 40, and 60 W/gU. This was done for the expected life of the fuel or three years. Below you can see the resulting swelling plots for both swelling versus time and burnup. A couple of notes, the fuel will now see the knee point within the life of the fuel. Also these fission rates are much lower than those used to develop and fit the model. Finally a figure showing the effect of the fission rate on the fission density at the knee is expanded to include these lower fission rates which are outside the range of the experimental data used to fit the model.

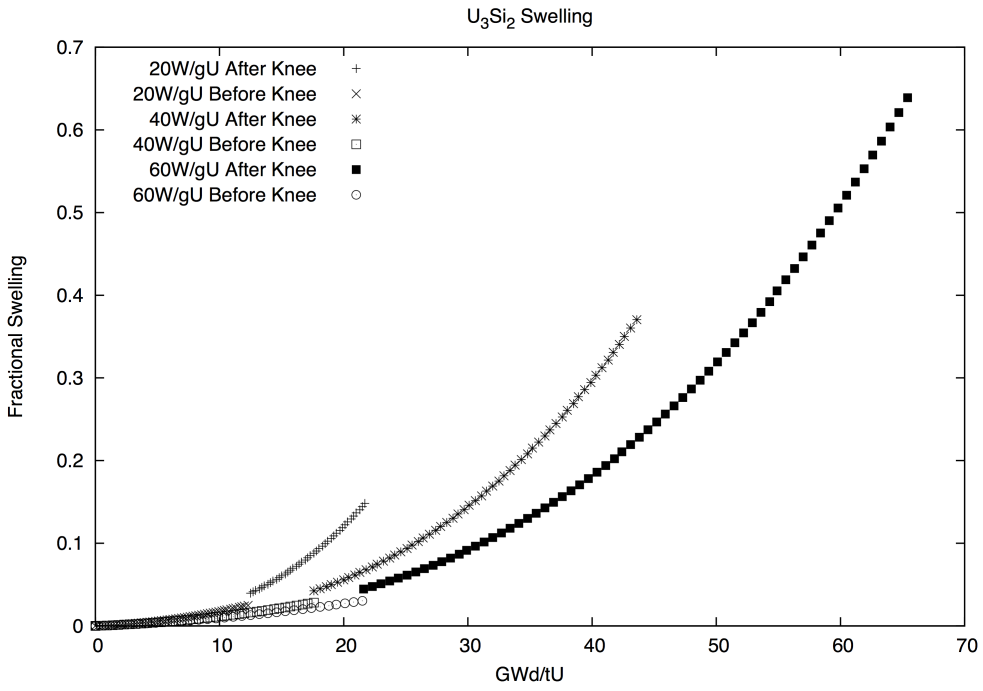

Figure 21: Fractional Swelling vs GWd/tU for U_3Si_2 for Reduced Fission Rates

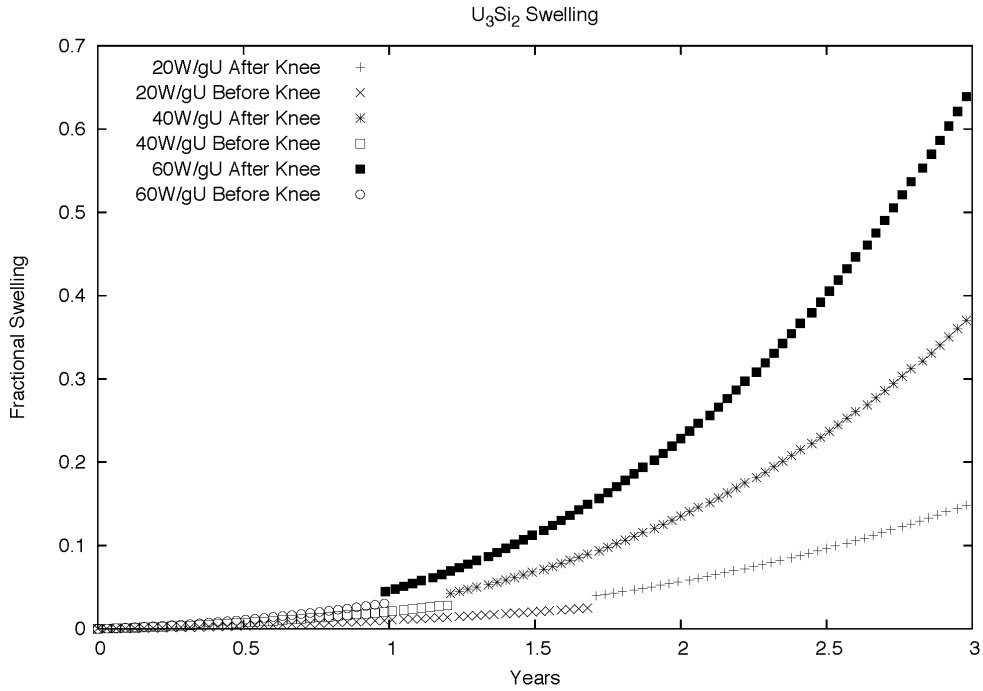

Figure 22: Fractional Swelling vs Time for U_3Si_2 for Reduced Fission Rates

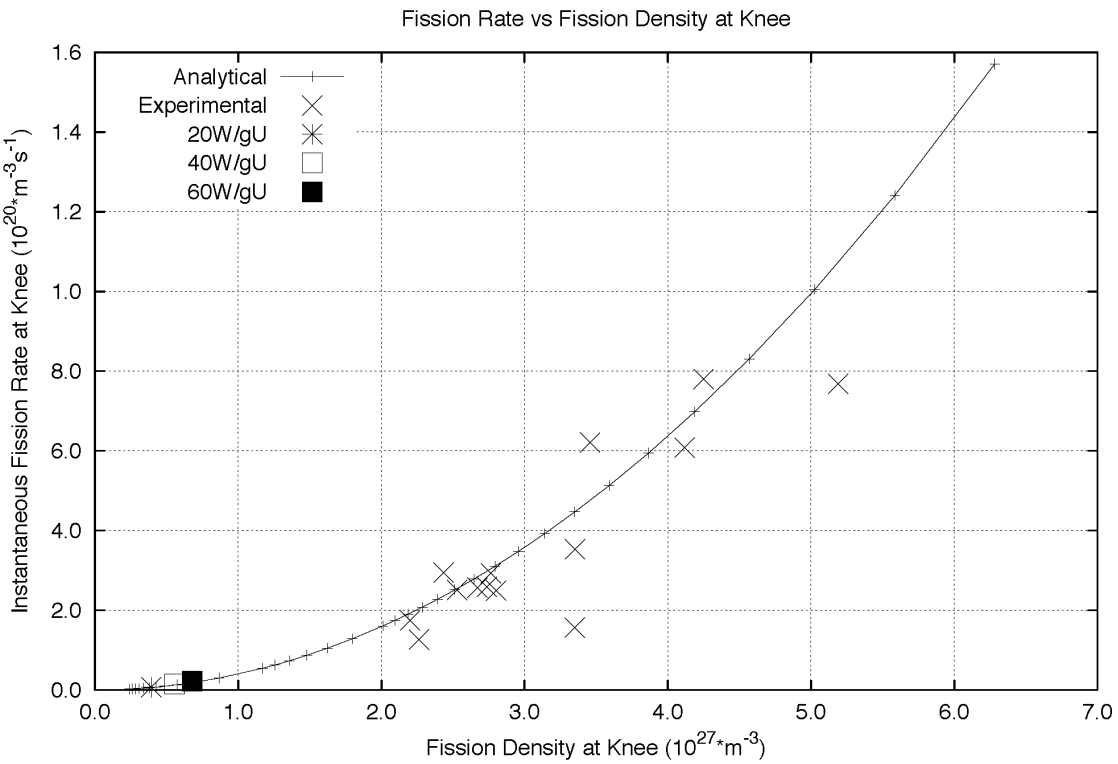

Figure 23: Fission Rate vs Fission Density at Knee: Comparison of Experimental, Analytical Values, and Reduced Fission Rates

During a simulation with BISON at a lower fission rate, Metzger calculated the swelling versus burnup for U_3Si_2[17]. This was done with an empirical expression. This equation was developed from data generated by Finlay[4] from irradiated aluminum dispersed mini-plate fuel. It should also be noted that the data was for burnups below 2×10^{27} fissions m^{-3}, of the same order as this work. The equation is shown below. The BISON code expression results in 0.019 V/V_o swelling at 20 GWd/tU for U_3Si_2 and 0.0125 V/V_o for UO_2. This corresponds to about 6.3×10^{26} fissions m^{-3} and 5.37×10^{26} for U_3Si_2 and UO_2 respectively. For the U_3Si_2, the model here results in 0.0123 V/V_o (it should be noted the swelling rates for different fission rates don't differ greatly until after the knee). The UO_2 fixed grain model results in 0.0117 V/V_o at 1500K (~875 hours).

$$\frac{V}{V_o}\% = \left(3.88008Bu^2 + 0.79811Bu\right) \times 100 \tag{54}$$

Note that in Eq. (54) burnup is in units MWd/tU. The table below shows the swelling at potential I2S-LWR burnups with both the empirical equation and the model from this paper.

Table 4: Empirical versus Model U_3Si_2 Swelling

	37 GWd/tU	46 GWd/tU
Developed Model	2.282%	2.970%
Empirical Relation (Eq. (54))	3.484%	4.492%

The fixed grain UO_2 model and U_3Si_2 model were used to compare the swelling of each fuel in the figure below. The swelling rate for U_3Si_2 is at least comparable to UO_2. Although U_3Si_2 becomes amorphous under irradiation, it is only amorphous up to 250°C[1] therefore the comparison had to be done at different temperatures. While amorphous the uniform distribution of bubbles helps to keep fission gases within the fuel for U_3Si_2, thereby preventing a pressure increase in the cladding plenum.

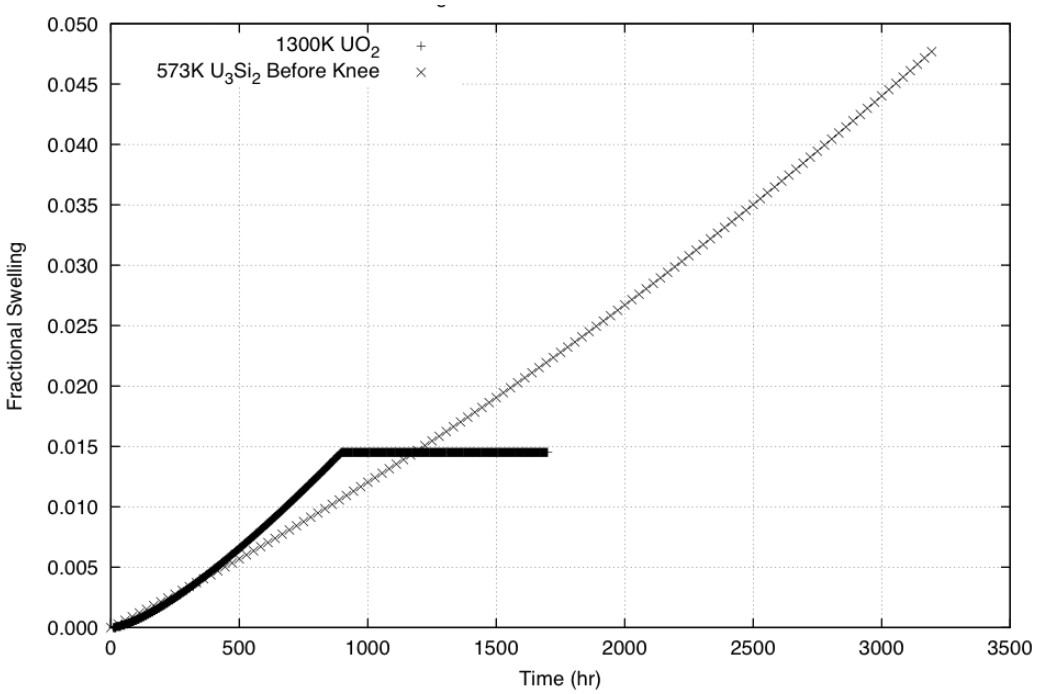

Figure 24: Swelling vs Time: Massih Fixed Grain (1300K) vs JRest (523K) UO_2 vs U_3Si_2 at 1.7×10^{20} $m^{-3}s^{-1}$ Fission Rate

For a more ideal comparison a model to evaluate U_3Si_2 swelling at higher temperatures while crystalline will be pursued. Developing a model to compare fission bubble formation and swelling for crystalline vs amorphous states for a given fuel would provide more insight into the differences for each. Initially, adapting the fixed grain model used with UO_2 will be pursued. To do this there are a number of parameters in the model specific to U_3Si_2 that will need to be updated to U_3Si_2. Unfortunately not all of these values are currently known, and until further experimental work is done to determine them the model would be at best an approximation. Table 5 below shows what values need to be adapted from UO_2 to U_3Si_2 to implement the fixed grain swelling model.

Table 5: Unknowns for U_3Si_2 Fixed Grain Swelling Model

Symbol	Description	Equation or Value for UO_2
D'	Diffusivity in a trap free media in UO_2	$C_1 e^{\frac{-Q_1}{k_b T}} + \dot{f} C_2 e^{\frac{-Q_2}{k_b T}} + C_3 \dot{f}$
C_b^t	Total bubble density	$\frac{1.52\times10^{27}}{T} - 3.3 \times 10^{23}$
$\bar{R}_b$	Intragranular bubble radius	$1.453 \times 10^{-10} \times e^{1.023\times10^{-3}T}$
r_{bs}	Average intergranular bubble radius at saturation	10^{-6} m
C_1	Constant	7.6×10^{-10}
C_2	Constant	4.5×10^{-35}
C_3	Constant	2×10^{-40}
Q_1/k_b	Activation Energy	35247 K
Q_2/k_b	Activation Energy	13800 K
L	Fission fragment range	6×10^{-6} m
δ	Damage radius of fission fragment	10^{-9} m

REFERENCES

[1] Birtcher, R. C., Richardson, J. W., and Mueller, M. H., "Amorphization of u3si2 by ion or neutron irradiation," *Journal of Nuclear Materials*, vol. 230, no. 2, pp. 158–163, 1996.

[2] Burke, J. E. and Turnbull, D., "Recrystallization and grain growth," *Progress in Metal Physics*, vol. 3, no. 0, pp. 220–292, 1952.

[3] Davies, D. and Long, G., "The emission of xenon-133 from lightly irradiated uranium dioxide spheroids and powders," Report AERE-R-4347 United KingdomMon Sep 10 07:19:36 EDT 2012DTIE; NSA-17-032563English, 1963.

[4] Finlay, M. R., Hofman, G. L., and Snelgrove, J. L., "Irradiation behaviour of uranium silicide compounds," *Journal of Nuclear Materials*, vol. 325, no. 2-3, pp. 118–128, 2004.

[5] Finlay, M. R., Hofman, G. L., Rest, J., Snelgrove, J. L., and San Carlos de Bariloche, A., "Behaviour of irradiated uranium silicide fuel revisited," 2002.

[6] Forsberg, K. and Massih, A. R., "Kinetics of fission product gas release during grain growth," *Modelling and Simulation in Materials Science and Engineering*, vol. 15, no. 3, pp. 335–353, 2007.

[7] Gibson, H. C., "Gaseous swelling and release in nuclear fuels during grain growth," 2013.

[8] Hofman, G., "A short note on high density dispersion fuel," 1996.

[9] Jernkvist, L. O. and Massih, A. R., "Models for fuel rod behaviour at high burnup," 2004.

[10] J.S. Rowlinson, B. W., "Molecular theory of capillarity," *Oxford University Press, Oxford, UK*, 1982.

[11] Maln, K., "Migration of i-131 in fuel rods with burn-ups of 5-30 mwd/kg u re-irradiated at power of 40-60 kw/m for up to five days," *Proc. Specialists' Mtg. Internal Fuel Rod Chemistry, IWGFPT/3*, p. 57, 1979.

[12] Massih, A. R. and Forsberg, K., "Calculation of grain boundary gaseous swelling in uo2," *Journal of Nuclear Materials*, vol. 377, no. 2, pp. 406–408, 2008.

[13] Massih, A. R., "Models for mox fuel behaviour," *A selective review, SKI Report*, vol. 10, 2006.

[14] Massih, A. R. and Jernkvist, L., "Nucleation and growth of second phase precipitates under non-isothermal conditions," *arXiv preprint cond-mat/0511201*, 2005.

[15] Matzke, H. J., "Gas release mechanisms in uo2, a critical review," *Radiation Effects*, vol. 53, no. 3-4, pp. 219–242, 1980.

[16] Matzke, H., "On the rim effect in high burnup uo2lwr fuels," *Journal of Nuclear Materials*, vol. 189, no. 1, pp. 141–148, 1992.

[17] Metzger, K. E., Knight, T. W., and Williamson, R. L., *Model of U3Si2 Fuel System using BISON Fuel Code*. 2014.

[18] Olander, D., "Fundamental aspects of nuclear reactor fuel elements," Report TID-26711-P1; TRN: 08-019392 United States10.2172/7343826TRN: 08-019392Fri Oct 10 17:18:32 EDT 2014Dep. NTISTIC; ERA-02-000713; EDB-76-080581English, 1976.

[19] Petrovic, B., Franceschini, F., and Ferroni, P., "Fuel cycle cost trade-off studies for i2s-lwr (integral inherently safe lwr) fuel design selection," 2014.

[20] Rest, J., "A model for fission-gas-bubble behavior in amorphous uranium silicide compounds," *Journal of Nuclear Materials*, vol. 325, no. 2-3, pp. 107–117, 2004. 773FJ Times Cited:5 Cited References Count:15.

[21] Rest, J. and Hofman, G. L., "Dynamics of irradiation-induced grain subdivision and swelling in u3si2 and uo2 fuels," *Journal of Nuclear Materials*, vol. 210, no. 1-2, pp. 187–202, 1994.

[22] Rest, J. and Hofman, G. L., "An alternative explanation for evidence that xenon depletion, pore formation, and grain subdivision begin at different local burnups," *Journal of Nuclear Materials*, vol. 277, no. 2-3, pp. 231–238, 2000.

[23] Speight, M., "A calculation on the migration of fission gas in material exhibiting precipitation and re-solution of gas atoms under irradiation," *Nuclear Science and Engineering*, vol. 37, no. 2, pp. 180–185, 1969.

[24] Turnbull, J. A., Friskney, C. A., Findlay, J. R., Johnson, F. A., and Walter, A. J., "The diffusion coefficients of gaseous and volatile species during the irradiation of uranium dioxide," *Journal of Nuclear Materials*, vol. 107, no. 2-3, pp. 168–184, 1982.

[25] White, R. J. and Tucker, M. O., "A new fission-gas release model," *Journal of Nuclear Materials*, vol. 118, no. 1, pp. 1–38, 1983.